Advances in Nano Research, *Vol. 12, No. 6 (2022) 583-592*
https://doi.org/10.12989/anr.2022.12.6.583

An experimental study on the picosecond laser dressing of bronze-bonded diamond wheels

Yanyi Wang[1,2], Genyu Chen*[2], Bang Hu[1,2] and Wei Zhou[1,2]

[1]*State Key Laboratory of Advanced Design and Manufacturing for Vehicle Body, Hunan University, Changsha 410082, China*
[2]*Laser Research Institute, Hunan University, Changsha 410082, China*

(*Received December 21, 2021, Revised March 11, 2022, Accepted March 13, 2022*)

Abstract. In this paper, a pulsed picosecond laser dressing method for bronze-bonded diamond wheel is studied systematically and comprehensively. The picosecond laser pulse ablation experiment is carried out, and the ablation thresholds of bronze-bonded and diamond abrasive particle are measured respectively. The results indicate that the single-pulse ablation thresholds of bronze-bonded are 0.89J/cm^2, 0.24J/cm^2 during strong/weak ablation stages. And the multi-pulse ablation thresholds of diamond abrasive particle are 1.69J/cm^2, 0.49J/cm^2 during strong/weak ablation stages. Obviously, diamond grains have less thermal damage during the process of gentle ablation. The diamond grains of the grinding wheel surface are graphitized during laser dressing. The bronze-bonded is relatively smooth and organizational stability, and the diamond grits have suitable prominent height, which are beneficial to maintain the good grinding performance of dressed bronze-bonded diamond grinding wheels.
Keywords: ablation thresholds; dressing; diamond grinding wheel; picosecond laser

1. Introduction

Hard and brittle materials, such as engineering ceramics, optical glass and hard alloy, have been widely used in all kinds of key equipment, and the grinding process of various complex surface parts has gradually increased(Shariati *et al*. 2012, 2016a, b, 2019, 2020d, e, f, g, h, i, j, 2021a, b, Dai and Safarpour 2021, Forsat *et al*. 2021, Ghamkhar *et al*. 2021, Khadimallah *et al*. 2021a. b, Kumar *et al*. 2021, Madenci 2021, Tlidji *et al*. 2021). Because of the advantages of high bond strength, good thermal conductivity, good wear resistance, long service life, and heavy load grinding, bronze diamond grinding wheel is widely used in shaping grinding, precision grinding and ultra-precision grinding of hard and brittle materials (Habibi *et al*. 2016, 2018a, b, 2019b, d, e, Ebrahimi *et al*. 2019a, Esmailpoor Hajilak *et al*. 2019, Pourjabari *et al*. 2019, Safarpour *et al*. 2019a). Bronze-bonded diamond grinding wheels are fabricated by sintering using diamond (the hardest material in the world) as an abrasive and bronze as a bonding material (Habibi *et al*. 2017, 2019a, c, Safarpour *et al*. 2018, 2019b, 2020, Alipour *et al*. 2020, Ebrahimi *et al*. 2020a, Ghazanfari *et al*. 2020, Chen *et al*. 2022). These grinding wheels exhibit excellent grinding performance and strong wear resistance and, therefore, do not need frequent dressing (Dold *et al*. 2011, Adamian *et al*. 2020, Al-Furjan *et al*. 2020a, b, Li *et al*. 2020b, Liu *et al*. 2020b, 2021b, Zare *et al*. 2020, Dai *et al*. 2021b, Habibi *et al*. 2021, He *et al*. 2021, Huang *et al*. 2021a, Zhang *et al*. 2021). However, dressing is required to produce or restore the wheel geometry and topography after the initial installation or if the wheel is blunted through using (Walter *et al*. 2012, Warhanek *et al*. 2015). Dressing a bronze-bonded diamond wheel consists of two processes: profiling and sharpening. Profiling is achieved by micro-cutting on ion and contour. Sharpening is achieved by "reroughening" the profiled grinding wheel surface by removing the bond around the abrasive grains, thereby generating inter abrasive chip space and ensuring that the abrasive protrudes at a proper height (the grain protrusion height in coarse-grained grinding wheels is usually tens of microns) (Chen *et al*. 2015). For grinding wheels with complex surface topographies and extremely high material strengths and hardness values, conventional "hard-on-hard" mechanical methods result in large dresser wear and only provide low dressing accuracy/efficiency (Ding *et al*. 2017). Pulsed-laser dressing technology is a non-contact method with a high flexibility that can completely prevent dressing tool wear while directly removing the diamond grains and bronze bond in a controllable manner, thereby achieving adequate dressing precision for coarse-grained bronze-bonded diamond grinding wheels (especially form grinding wheels with complex curved surfaces) (Stompe *et al*. 2012, von Witzendorff *et al*. 2012, Lutey *et al*. 2016).

In laser dressing, an incident laser beam is focused on to the wheel surface to remove the surface material of the wheel through selective ablation, thus achieving the required dimension and contour accuracy of the grinding wheel, along with good surface topography(Ma *et al*. 2021, Zhao *et al*. 2021, Liu *et al*. 2020a, Wang *et al*. 2020, Zhou *et al*. 2020, Dai *et al*. 2021a, Guo *et al*. 2021a, Hou *et al*. 2021, Huang *et al*. 2021b, c, Jiao *et al*. 2021, Liu *et al*. 2021c, Moradi *et al*. 2021, Shao *et al*. 2021, Wu and Habibi 2021, Xu *et al*. 2021, Yu *et al*. 2022). When dressing the grinding wheel, the incident laser beam can originate from either the radial or tangential direction, as shown in Fig. 1. Research studies to date have consisted of experimental

*Corresponding author, Professor,
E-mail: hdgychen@163.com

ISSN: 2287-237X (Print), 2287-2388 (Online)

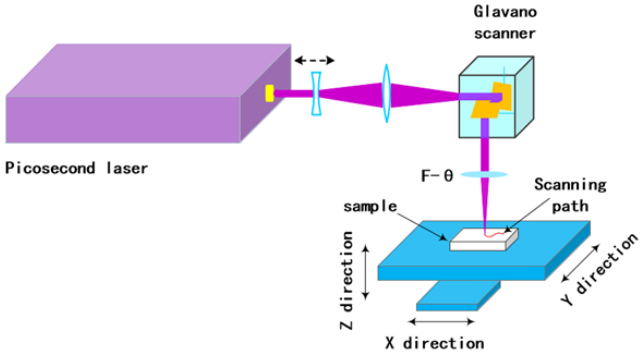

Fig. 1 Scheme of the experimental setup

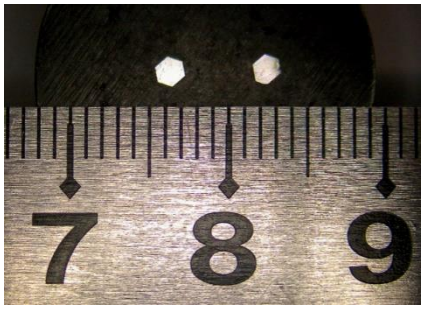

Fig. 2 Diamond insert sample

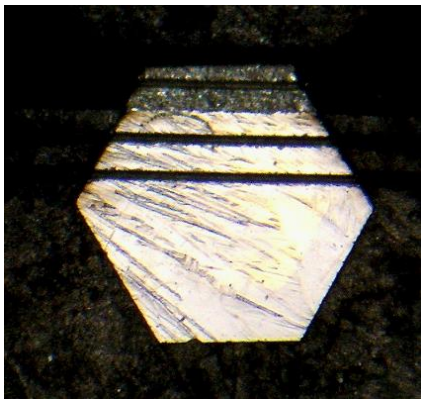

Fig. 3 Effect of diamond scribing test

investigations of radial laser dressing technologies, e.g., the studies performed at the Institute of Laser Technology, Hunan University (Zahedi *et al*. 2014, 2015, Boerner *et al*. 2015, Azarhoushang and Zahedi 2017), the Institute of Machine Tools and Manufacturing, the Swiss Federal Institute of Technology (ETH) Zurich (Jaeggi *et al*. 2011), and the Laser Zentrum Hannover e.V. (Jeschke *et al*. 2002, Zahedi *et al*. 2015). Instead of performing precision profiling, a radial laser beam only sharpens the grinding wheel because the size of the laser beam cross-section along the direction of light propagation and the laser energy distribution over this cross-section change continuously (Ebrahimi *et al*. 2019b, c, Hashemi *et al*. 2019, Moayedi *et al*. 2019, 2020a, b, Mohammadgholiha *et al*. 2019, Mohammadi *et al*. 2019, Ebrahimi *et al*. 2020b, Habibi *et al*. 2020, Oyarhossein *et al*. 2020, Shariati *et al*. 2020a, b, Shokrgozar *et al*. 2020). Moreover, there is no definitive "knife tip" position for the laser beam, i.e., the laser energy is continuous in the incident direction. Thus, when the laser beam scans the wheel surface, the beam tends to remove the wheel surface material randomly. In addition, the removal depth cannot be easily controlled. Therefore, this dressing method cannot be used to correct contour errors of the wheel, or to obtain the required dimensional accuracy of the wheel, i.e., precision profiling cannot be achieved. This issue results in a bottleneck in laser dressing technology.

To address this problem, we develop a new grinding wheel profiling method using online laser sharpening. In this study, online laser sharpening experiments were conducted on coarse-grained bronze-bonded diamond wheels using a pulsed picosecond laser. The surface micro-morphology, the circular runout error, the axial gradient error of the profiled wheel, and the degree of graphitization of the diamond grains were measured.

In order to get a better surface, basic research on ablation behavior of pulse ablation bronze bond and diamond abrasive grain must be carried out. Pulse laser radial cutting diamond grinding wheel, in essence, is the process of multi pulse ablation of the binder on the surface of the grinding wheel by the ablation pits formed by the laser pulse sequence. In the process of laser sharpening, it is necessary to effectively remove the binder and not damage the abrasive particles, while the diamond abrasive particles are prone to produce metamorphic layer and micro crack under the heat action. It is necessary to optimize the selection of pulse energy. In this chapter, the ablation threshold test of picosecond laser bronze bond and diamond abrasive will be carried out respectively, and the pulse ablation threshold of bronze bond and diamond abrasive will be measured by experiments.

2. Experimental apparatus and method

Fig. 1 is a schematic of the online laser dressing system. The mean power (Pavg) of the pulsed picosecond laser is 30–100 W, the pulse repetition frequency (f) is 400 kHz, and the pulse width (τ) is 10 ps. The laser beam is transmitted by a single-mode into an ablation head, which is fixed on a motorized three-dimensional (3D) translation stage, and then collimated, shaped, focused, and tangentially directed onto the surface of the grinding wheel (diameter D=100 mm, width W=10 mm, grain size 120#) that is mounted on the spindle of a precision surface grinder. The beam spot of the square-shaped top-hat beam on the grinding wheel surface is dimensions of 35×35 μm. The rotational speed (n) of the grinding wheel is set at 300 rpm.

Diamond grains are usually irregular polyhedral, and fixtures are not easy to clamp. It is necessary to carry out an exploratory test of a certain surface of the fixed diamond polyhedron when the interaction between diamond and laser is studied, the incidence angle and the amount of defocus are greatly influenced. Therefore, a large size, single crystal diamond without impurities is inserted into a clean surface, the insert sample is shown in Fig. 2. The highest temperature of the mounting presses only 130, which will not destroy the properties of diamond. In order to avoid the effect of dust and other impurities on the observation effect before the diamond scanning test is carried out, the

Table 1 Varied parameters of ps-laser ablation

Average power P	Scanning speed v_s	Repetition rate f	Number of scans N_s
30 ~ 100W	0 ~ 20 m/s	0.4 ~ 2MHz	1 ~ 10

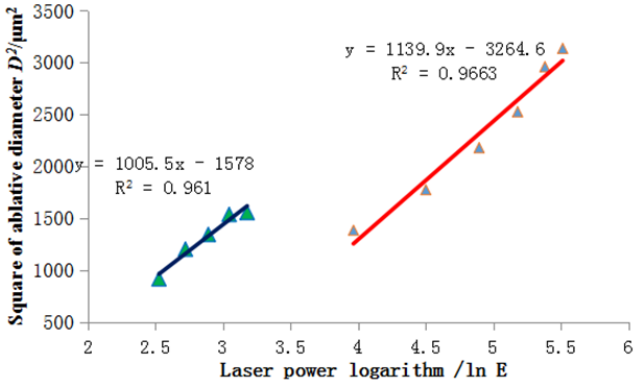

Fig. 4 The relationship between the diameter of the ablation zone and the logarithm of the pulse energy

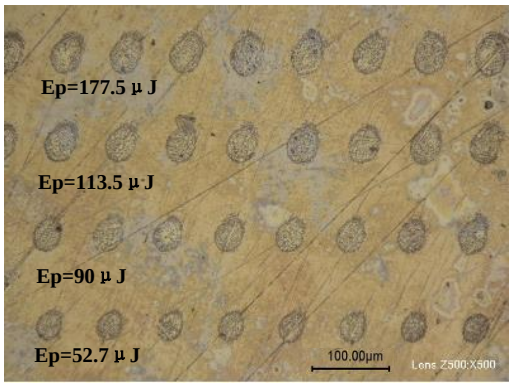

Fig. 5 Monopulse with different pulse energy of bronze bond

ultrasonic cleaning is carried out after 5 minutes and then dried. The effect of picosecond laser scribing test is shown in Fig. 3. The visible stage is reasonable, and the ablation surface is easy to observe.

During dressing, the 3D translation stage is adjusted to move the ablation head down to a set distance (ar=30μm), i.e., the cutting depth of the laser beam. Meanwhile, the laser ablation head scanned the contour line of the grinding wheel in cycles at a constant speed (v) of 30μm/s. The abrasive and the bond that interfered with the laser beam are removed by the laser. A laser beam power meter is simultaneously used for the online monitoring of the power of the part of the beam that is transmitted through the wheel surface, i.e., the part of the beam that don't contact the materials on the wheel surface. If the measured power reaches a preset threshold value (80 % of Pavg), then the laser ablation head move down a distance, and the dressing continued.

3. Results and discussion

Experimental measurement of ablation threshold of picosecond laser ablation bronze bond is presented in Table 1.

In this part, the ablation threshold of bronze bond will be measured by experimental method. The measurement methods of the ablation threshold include plasma radiation, damage detection, extrapolation (volume calculation and area pushing algorithm), extrapolation, especially the area push algorithm, and the area of the ablative pit is convenient to measure, and the precision is high and the application is wide. Therefore, the area estimation method is used to test the ablation threshold. The energy of pulsed laser is Gauss distribution, and its energy distribution satisfies the following relations.

$$I(\mathrm{r}) = I_0 e^{-\frac{2r^2}{\omega_0^2}} \tag{1}$$

In the formula, ω_0 is the waist radius of the beam, r is the distance from the center of the beam, and I_0 is the peak power density of the laser. The diameter of the blind hole formed on the surface of the material is also different when the energy density (Hashemi *et al*. 2019, Al-Furjan *et al*. 2020c, d, e, f, Bai *et al*. 2020, Cheshmeh *et al*. 2020, Li *et al*. 2020a, Lori *et al*. 2020, Najaafi *et al*. 2020, Shariati *et al*. 2020c, Xiong *et al*. 2020, Guo *et al*. 2021b, Liu *et al*. 2021a) is different. In an ablation zone with a diameter of D, the energy density of the outer contour is that the laser can ablate the boundary energy of the material, and there is a relationship between the diameter and the laser energy density:

$$I_{th} = I_0 e^{-\frac{D^2}{2\omega_0^2}} \tag{2}$$

In the formula, the I_{th} is the ablation threshold, and the D is the diameter of the blind hole. The peak power density of laser can be calculated by the following formula:

$$I_0 = \frac{2E_P}{\tau\pi\omega_0^2} \tag{3}$$

E_p is a single pulse energy, and the above formula can be obtained:

$$I_{th} = \frac{2E_P}{\tau\pi\omega_0^2} \cdot e^{-\frac{D^2}{2\omega_0^2}} \tag{4}$$

$$D^2 = 2\omega_0^2 \ln E_P - 2\omega_0^2 \ln E_{th} \tag{5}$$

Type (5) is a straight line about which the slope is. Through the experiment, the relation curve of the square of the diameter of the ablation pit and the pulse energy is fitted out as shown in the following diagram (the linear equation is fitted by the logarithm of the least square method, in which the R^2 shows the degree of data consistency).

According to the definition of the ablation threshold, the values of the external D=0 are: E_{ths}(1)=17.5μJ and E_{thg} (1)=4.8μJ, in which E_{ths}(1) and E_{thg} (1) are the single pulse energy ablation threshold of the strong / weak ablation stage. The energy density ablation threshold can be obtained by the following calculation:

$$F_{th} = \frac{2E_{th}}{\pi\omega_0^2} \tag{6}$$

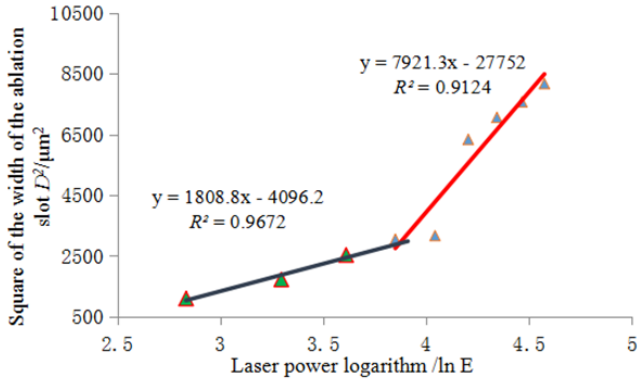

Fig. 6 The relation between the square of the width of the diamond ablation slot and the logarithm of the pulse energy

The calculation results are as follows: $F_{ths}(1)$=0.89 J/cm^2 and $F_{thg}(1)$=0.24 J/cm^2, where $F_{ths}(1)$ and $F_{thg}(1)$ are strong / weak ablation stage bronze monopulse energy density ablation threshold. As shown in Fig. 5, the pulse ablation effect is different for different pulse energies. It can be seen that the diameter of different monopulse energy is different. As the energy of monopulse increases, the ablation area becomes larger. Due to the short action time, a deep level ablation pit is formed. The ablation area is elliptical and not standard, because the beam quality is lossy during the beam propagation.

With the increase of laser pulse times, the ablation threshold of multi pulse is smaller than that of single pulse ablation. Moreover, when the number of pulses increases further, the change trend of ablation threshold of multiple pulses slows down, and eventually becomes stable at a certain value. The relationship between single pulse and multi pulse ablation threshold can be described as follows:

$$F_{th}(N) = F_{th}(1) * N^{(\xi-1)} \tag{7}$$

The energy density ablation threshold of pulse number is N and 1, respectively, to describe the influence factor of thermal accumulation. And the multi pulse threshold of copper binder is measured. When the number of pulse is 313, the ablation threshold of the copper bond energy density is $F_{th}(313)$=0.75 J/cm^2. When the pulse number is 1270, the ablation threshold of bronze bond energy density is $F_{th}(1270)$=0.6 J/cm^2. It can be seen that with the increase of pulse number, thermal accumulation becomes larger and the ablation threshold of bronze bond gradually decreases.

The nanosecond fiber pulse laser (f=50 KHz, τ=210 ns, λ=1064 nm) is used to measure the single pulse threshold $F_{th}(1)$=2.26 J/cm^2 of bronze binding agent, which is close to that of $F_{th}(1)$=2.96 J/cm^2. The ablation threshold of nanosecond laser bronze bond is larger than that of picosecond laser ablation threshold. It can be seen that with the decrease of nanosecond to picosecond pulse width, the ablation threshold of bronze bond has been reduced. In order to verify the correctness of the results, consult related literature. The Ali Zahedi research group of German University of Applied Science, Germany, shows that the metal binding agent E_{th}=12.5 μJ is slightly smaller than the experimental results. The reason may be: the research group of the picosecond laser pulse width of τ <10 ps, with smaller than the test. The pulse width is smaller and closer to the "cold processing" effect, and material removal is easier.

There are few literatures on the effect of picosecond laser on bronze binder. The bronze binder is mainly sintered from copper powder. There are many studies on the effect of picosecond laser or femtosecond laser on pure copper. The Paul Boerner and others of Swiss Confederation Polytechnic Institute, from the extrapolation method, obtained the multi pulse $F_{th}(100)$=0.23 J/cm^2 (τ =10 ps, λ=532 nm, f =50 kHz) by extrapolation, and the possible reason is that the absorption rate of the laser beam in the ultraviolet band is greater than the infrared band for the copper material. The Lithuania Institute of physical application, Gediminas Raciukaitis *et al*. (2021), obtained the single pulse ablation threshold of pure copper by extrapolation, $F_{th}(1)$=1.73 J/cm^2 (τ =10 ps, D=20 μm, λ =1064 nm, f =1 kHz). This test is out slightly, the reasons may be: picosecond laser models are not the same, and not the same as the beam quality factor. Jaeggi, Berne University of Applied Sciences, Switzerland, and others, obtained the single pulse ablation threshold of pure copper by extrapolation, F_{th}=0.95 J/cm^2 (τ =10 ps, D=35 μm, λ=1064 nm, f =50 Hz). The results are close to the results of this test.

Diamond is a hard and brittle material with high reflectivity and high refractive index. If a single pulse acts on it, it will not be convenient to observe its ablation effect due to the severe loss of the laser itself. At the same time, it is difficult to study the single pulse ablation threshold for high frequency pulse laser. It is a feasible method to study the surface ablation threshold by using overlapping pulse laser to scan the diamond abrasive particles. Here, the concept of effective pulse number is introduced, that is, the energy accumulated by Gauss pulsed laser beam is equal to that during static ablation process when the groove is scribed. The relationship between effective pulse number and laser scanning speed v, spot diameter D and repetition frequency f is as follows:

$$N = \sqrt{\frac{\pi}{2}} \cdot \frac{Df}{2v} \tag{8}$$

In the experiment, the repetition frequency f=2 MHz, the scanning speed v=8 m/s, the spot diameter of D=50 μm, scanning 1000 times, can obtain the effective pulse number N=3133, the laser beam which only changes the single pulse energy is scanned, and the relationship between the slot width and the laser energy is obtained. As shown in Fig. 6, the linear equation is fitted by the least square logarithm, of which R^2 is shown. Indicating the degree of conformity of the data). According to the definition and formula of ablation threshold (5), when D=0 is launched, the value of E_P are $E_{thg}(3133)$=9.6 μJ and $E_{ths}(3133)$=33.2 μJ. Among them, $E_{thg}(3133)$ represents the weak ablation stage, the multi pulse energy ablation threshold of diamond abrasive particles, $E_{ths}(3133)$ represents the strong ablation stage, the multi pulse energy ablation threshold of the diamond abrasive particles, and can be calculated to be $F_{thg}(3133)$=0.49 J/cm^2 and $F_{ths}(3133)$=1.69 J/cm^2.

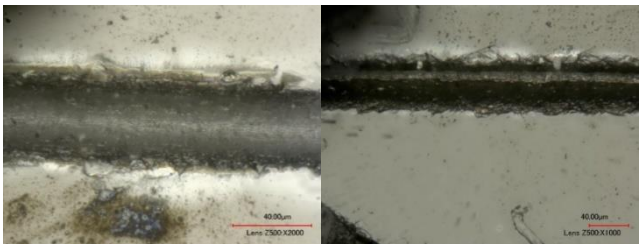

(a) E_P=27 μJ (b) E_P=57 μJ

Fig.7 Energy ablation effect of different monopulse

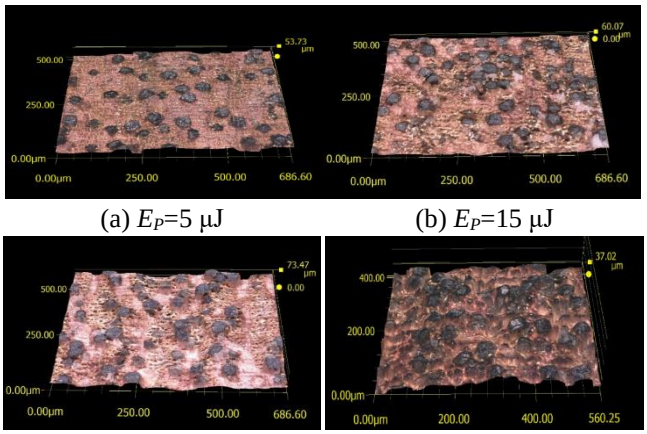

(a) E_P=5 μJ (b) E_P=15 μJ

(c) E_P=25 μJ (d) E_P=35 μJ

Fig. 8 Different laser monopulse energy grinding wheel morphology

In order to verify the correctness of the test results, consult related literature. The German University of Applied Sciences Ali Zahedi research group, line scan to obtain experimental results of diamond grits E_{th}=37.5 μJ. The ablation threshold of the experimental results in strong erosion stage and test results slightly smaller, but the basic approach. In the weak ablation stage, Ali Zahedi research group did not analyze. When the energy of the incident pulse is low, the width of the slot obtained by the scanning line changes slowly with the logarithm of the pulse energy, as shown in the blue fitting line in Fig. 6. Under the condition of higher pulse energy, the width of the slot changes faster with the logarithm of the pulse energy, as shown in the red fitting line at the beginning of Fig. 6. The two ablation stages can be defined as weak ablation and strong ablation.

The mechanism of material removal is different from two stages of weak ablation and strong ablation. Different ablation grooves are obtained by scanning line, the integrity of the edge of the groove (the effect of diamond crack), the size of the heat affected zone, the color of the surface, and so on, can reflect the intensity of the ablation, which is related to the different ablation stages (different pulse energy). As shown in Fig. 7(a), the weak ablative stage, although the magnification is 2000 times, the edge crack is less, the edge integrity is better, the edge of the groove has a small amount of white area, the white area has a small number of cracks and the crack size is less than 20μm after the use of high power lens. Diamond is a hard brittle material, but the energy of laser monopulse is low, the ablation is weak, and in the weak ablation stage, evaporation is the main factor, and the force of diamond is smaller and the crack is less. As shown in Fig. 7(b), at this stage, the color of the groove surface is deeper than that of the non-ablated area, indicating that the groove surface structure has changed. In the strong ablative stage, the edge cracks are obvious, the edge integrity is poor and the irregular gaps are visible, there are a small number of white areas on the edge of the trough, the lower edge is few or no, but the lower edge is denser. Due to the high energy of the pulse laser and the stress concentration, the cracks in the lower edge have completely cracked, the material is removed irregularly, and mainly by “phase explosion” removal, resulting in the gap as shown in the diagram. Compared with Figs. 7(a) and 7(b), the color of the groove surface is deeper. Diamond has also undergone structural change, and graphitization is obvious. When the laser pulse energy is too large, the stress concentration causes the large area of diamond surface to fall off. It provides a strong argument for the above discussion process.

Under the experimental conditions, the laser spot diameter is certain, and the laser pulse energy is one to one with the laser energy density. Laser pulse energy is a key parameter during pulsed laser dressing. The value of laser pulse energy affects not only the smoothness of binder, but also the thermal damage after abrasive ablation. The integrity of the diamond grinding particles after ablation is mainly considered, that is, when the grinding edge is sharp and the heat damage is small, the overall evenness of the binder is guaranteed, which is the standard to determine the appropriate laser single pulse energy.

In Fig. 8, the ablation profile of the laser scanning path line is L_1=15 μm, the laser beam scanning speed is v=4 m/s, the laser repetition rate is f=2 MHz, and the laser scanning times is N=30, under the different laser single pulse energy conditions, the surface of the bronze bonded diamond abrasive layer. As in Fig. 8(a), when the laser single pulse energy is E_P=5 μJ, the thresholds of the weak ablation stage of the bronze bond and the diamond (4.8 μJ and 9.6μJ respectively), the diamond abrasive particles are more complete, but the abrasive grains are basically without the outstanding height, and the material is mainly removed by evaporation. From Fig. 8(a), we can see that there are only a few bronze bonds on the surface of the wheel being gasified, and the bronze bond is not effectively removed.

In Fig. 8(b), when E_P=15 μJ, it is a little smaller than the threshold of 17.5 μJ in the strong ablation stage of bronze. The bronze bond is in weak ablation stage, but the ablation rate is increasing. Less than 33.2 μJ, the diamond has no obvious thermal damage. At this time, the diamond abrasive grain integrity is good, and the abrasive grain outburst is effectively highlighted. The bronze bond is removed effectively, and a small amount of bronze bond melt is found on the surface of the grinding wheel. The bronze binder basically keeps its original color and has little heat influence. When E_P=20 μJ (greater than 17.5 μJ), the bronze binder is in a strong ablation stage, the color of the surface of the grinding wheel becomes deeper and the bronze binder presents light black, indicating that the ablation temperature is higher and the black molten copper oxide is formed. The surface shape of diamond grains is irregular,

due to the large heat effect and high ablation temperature, and the defects such as breakage and corner loss on the abrasive grains. At the same time, the height of the protruding particle is larger, and some abrasive grains have already fallen off. The heat damage of these abrasive particles is very bad for grinding the workpiece, it is easy to produce the breakage of abrasive particles and the falling defects of the abrasive particles. These defects will accelerate the grinding wheel wear. With the increasing of laser pulse energy, the thermal damage of diamond wear and tear is becoming more and more serious. When E_P=35 μJ, in the right map of Fig. 8(d), red area are marked. Because of the large amount of debris falling off, the bond is ablated sharply, and a concave "basin" area has been produced, which has seriously damaged the structure of the grinding wheel and is not conducive to the grinding performance of the grinding wheel.

The scanning speed is different,the number of effective pulses in single channel scanning is different. That is to say, the number of multiple pulses is different. The scanning speed is reduced from 6 m/s to 0.5 m/s, and the corresponding effective pulse values are 125, 188, 376, 752 and 1504, respectively. In Fig. 8(a), the ablation zone has less laser pulse, and the surface bond of the grinding wheel has not been effectively removed, and the height of the abrasive grain is not enough and the space of the capacity is small. The height of the abrasive surface is not enough to achieve the purpose of grinding, and the grinding performance of the grinding wheel is poor. The small volume of abrasive surface on the grinding wheel is easy to cause the grinding wheel blockage and the grinding force to increase. In Fig. 8(b), the abrasive grains are relatively complete and high enough. With the decrease of laser beam scanning speed, the number of laser pulses increased on the unit area of the grinding wheel, and the number of effective pulses increased to 376. From the fourth chapter, we know that the bronze bond F_{th}(313)=0.75 J/cm^2, while the E_P=15 μJ corresponds to the energy density of 0.76J/cm^2, which is larger than the ablation threshold. Therefore, when the laser beam scanning speed changes to v=2 m/s, the heat accumulation of the unit ablation area becomes larger, the surface color of the bronze binder and the abrasive particles becomes deeper, and the copper binder surface produces copper oxide, and it is relatively rough. At the same time, some of the abrasive particles have fallen off. In Fig. 8(d), the binder has been ablated violently, and the molten binder has even been wrapped in the abrasive particles, and some of the abrasive particles are shedding, and the surface of the grinding wheel is very rough. At this time the grinding wheel is basically not grinding. In Fig. 8, the number of effective pulses is 1504, and the bronze binder F_{th}(1270) =0.6 J/cm^2 of the fourth chapter, and the pulse number of 1504, the bronze binder threshold is smaller than the 0.6 J/cm^2. The ablation threshold continues to be smaller, which leads to the deeper color of the binder, and the surface of the grinding wheel is covered with fused black copper oxide, and the surface structure of the grinding wheel has been changed and extremely rough, so it can not be used for grinding. This is because the ablation threshold of the bond and the diamond particles will become smaller as the heat accumulation of the unit ablation area becomes larger, the number of effective pulses is more, and the ablation threshold of the bond and the diamond abrasive will become smaller.

To sum up, when the laser single pulse energy is E_P=15 μJ, the average roughness of the bronze binders has little change, the average roughness is small, the heat effect is small, the integrity of the diamond grit is better, and the gold rigid sand wheel with good topography and geomorphology can be obtained.

4. Conclusions

The Experiments on picosecond laser ablation of bronze bond show that the single pulse energy density ablated F_{ths}(1)=0.89 J/cm^2 and F_{thg}(1)=0.24 J/cm^2 in strong / weak ablation stage. The threshold value of multi pulse threshold energy density of bronze bond is F_{th}(313)=0.75 J/cm^2 and F_{th}(1270)=0.6 J/cm^2. By using picosecond laser scanning method, the ablation diamond abrasive particles are obtained: the multi pulse energy density threshold of the strong / weak ablation stage is F_{ths}(3133)=1.69 J/cm^2 and F_{thg}(3133)=0.49 J/cm^2 respectively. The effect of scanning and Scribing on two stages of strong / weak ablation is analyzed. In the weak ablation stage, the cracks of diamond abrasive particles is less, the edge contour integrity is good, the material removal is mainly evaporation, and the diamond abrasive grains are very serious and the edge gap is more notched in the strong ablation stage, and the material removal is mainly phase explosion. In order to obtain good abrasive grains, strong abrasive erosion should be avoided.

Acknowledgement

The authors are grateful for the financial support from the National Science and Technology Major Project of the Ministry of Science and Technology of the People's Republic of China (No.2012ZX04003101).

References

Adamian, A., Safari, K.H., Sheikholeslami, M., Habibi, M., Al-Furjan, M. and Chen, G. (2020), "Critical temperature and frequency characteristics of GPLs-reinforced composite doubly curved panel", *Appl. Sci.*, **10**(9), 3251. https://doi.org/10.3390/app10093251.

Al-Furjan, M., Dehini, R., Khorami, M., Habibi, M. and won Jung, D. (2020a), "On the dynamics of the ultra-fast rotating cantilever orthotropic piezoelectric nanodisk based on nonlocal strain gradient theory", *Compos. Struct.*, 112990. https://doi.org/10.1016/j.compstruct.2020.112990.

Al-Furjan, M., Fereidouni, M., Habibi, M., Abd Ali, R., Ni, J. and Safarpour, M. (2020b), "Influence of in-plane loading on the vibrations of the fully symmetric mechanical systems via dynamic simulation and generalized differential quadrature framework", *Eng. Comput.*, 1-23. https://doi.org/10.1007/s00366-020-01177-7.

Al-Furjan, M., Fereidouni, M., Sedghiyan, D., Habibi, M. and won Jung, D. (2020c), "Three-dimensional frequency response of the

CNT-Carbon-Fiber reinforced laminated circular/annular plates under initially stresses", *Compos. Struct.*, 113146. https://doi.org/10.1016/j.compstruct.2020.113146.

Al-Furjan, M., Habibi, M., won Jung, D. and Safarpour, H. (2020d), "Vibrational characteristics of a higher-order laminated composite viscoelastic annular microplate via modified couple stress theory", *Compos. Struct.*, 113152. https://doi.org/10.1016/j.compstruct.2020.113152.

Al-Furjan, M., Moghadam, S.A., Dehini, R., Shan, L., Habibi, M. and Safarpour, H. (2020e), "Vibration control of a smart shell reinforced by graphene nanoplatelets under external load: Semi-numerical and finite element modeling", *Thin Wall. Struct.*, 107242. https://doi.org/10.1016/j.tws.2020.107242.

Al-Furjan, M., Oyarhossein, M.A., Habibi, M., Safarpour, H. and Jung, D.W. (2020f), "Frequency and critical angular velocity characteristics of rotary laminated cantilever microdisk via two-dimensional analysis", *Thin Wall. Struct.*, **157**, 107111. https://doi.org/10.1016/j.tws.2020.107111.

Alipour, M., Torabi, M.A., Sareban, M., Lashini, H., Sadeghi, E., Fazaeli, A., Habibi, M. and Hashemi, R. (2020), "Finite element and experimental method for analyzing the effects of martensite morphologies on the formability of DP steels", *Mech. Based Des. Struct.*, **48**(5), 525-541. https://doi.org/10.1080/15397734.2019.1633343.

Azarhoushang, B. and Zahedi, A. (2017), "Laser conditioning and structuring of grinding tools–a review", *Adv. Manufact.*, **5**(1), 35-49. https://doi.org/10.1007/s40436-016-0167-0.

Bai, Y., Alzahrani, B., Baharom, S. and Habibi, M. (2020), "Semi-numerical simulation for vibrational responses of the viscoelastic imperfect annular system with honeycomb core under residual pressure", *Eng. Comput.*, 1-26. https://doi.org/10.1007/s00366-020-01191-9.

Boerner, P., Zandonadi, G., Eberle, G. and Wegener, K. (2015). "Experimental and modelling investigations into the laser ablation with picosecond pulses at second harmonics", *Laser Based Micro Nanoproc. IX*, **9351**, 19-31. https://doi.org/10.3103/S1541308X18040027.

Chen, F., Chen, J., Duan, R., Habibi, M. and Khadimallah, M.A. (2022), "Investigation on dynamic stability and aeroelastic characteristics of composite curved pipes with any yawed angle", *Compos. Struct.*, 115195. https://doi.org/10.1016/j.compstruct.2022.115195.

Chen, G., Deng, H., Zhou, X., Zhou, C., He, J. and Cai, S. (2015), "Online tangential laser profiling of coarse-grained bronze-bonded diamond wheels", *Int. J. Adv. Manuf. Technol.*, **79**(9), 1477-1482. https://doi.org/10.1007/s00170-015-6963-z.

Cheshmeh, E., Karbon, M., Eyvazian, A., Jung, D.w., Habibi, M. and Safarpour, M. (2020), "Buckling and vibration analysis of FG-CNTRC plate subjected to thermo-mechanical load based on higher order shear deformation theory", *Mech. Based Des. Struct.*, 1-24. https://doi.org/10.1080/15397734.2020.1744005.

Dai, H. and Safarpour, H. (2021), "Frequency and thermal buckling information of laminated composite doubly curved open nanoshell", *Adv. Nano Res.*, **10**(1), 1-14. https://doi.org/10.12989/anr.2021.10.1.001.

Dai, Z., Jiang, Z., Zhang, L. and Habibi, M. (2021a), "Frequency characteristics and sensitivity analysis of a size-dependent laminated nanoshell", *Adv. Nano Res.*, **10**(2), 175-189. https://doi.org/10.12989/anr.2021.10.2.175.

Dai, Z., Zhang, L., Bolandi, S.Y. and Habibi, M. (2021b), "On the vibrations of the non-polynomial viscoelastic composite open-type shell under residual stresses", *Compos. Struct.*, 113599. https://doi.org/10.1016/j.compstruct.2021.113599.

Ding, W., Zhang, L., Li, Z., Zhu, Y., Su, H. and Xu, J. (2017), "Review on grinding-induced residual stresses in metallic materials", *Int. J. Adv. Manuf. Technol.*, **88**(9), 2939-2968. https://doi.org/10.1007/s00170-016-8998-1.

Dold, C., Transchel, R., Rabiey, M., Langenstein, P., Jaeger, C., Pude, F., Kuster, F. and Wegener, K. (2011), "A study on laser touch dressing of electroplated diamond wheels using pulsed picosecond laser sources", *CIRP Annals*, **60**(1), 363-366. https://doi.org/10.1016/j.cirp.2011.03.117.

Ebrahimi, F., Habibi, M. and Safarpour, H. (2019a), "On modeling of wave propagation in a thermally affected GNP-reinforced imperfect nanocomposite shell", *Eng. Comput.*, **35**(4), 1375-1389. https://doi.org/10.1007/s00366-018-0669-4.

Ebrahimi, F., Hajilak, Z.E., Habibi, M. and Safarpour, H. (2019b), "Buckling and vibration characteristics of a carbon nanotube-reinforced spinning cantilever cylindrical 3D shell conveying viscous fluid flow and carrying spring-mass systems under various temperature distributions", *Proceedings of the Institution of Mechanical Engineers, Part C: Journal of Mechanical Engineering Science*, **233**(13), 4590-4605. https://doi.org/10.1177/0954406219832323.

Ebrahimi, F., Hashemabadi, D., Habibi, M. and Safarpour, H. (2020a), "Thermal buckling and forced vibration characteristics of a porous GNP reinforced nanocomposite cylindrical shell", *Microsyst. Technol.*, **26**(2), 461-473. https://doi.org/10.1007/s00542-019-04542-9.

Ebrahimi, F., Mohammadi, K., Barouti, M.M. and Habibi, M. (2019c), "Wave propagation analysis of a spinning porous graphene nanoplatelet-reinforced nanoshell", *Wave. Random Complex Med.*, 1-27. https://doi.org/10.1080/17455030.2019.1694729.

Ebrahimi, F., Supeni, E.E.B., Habibi, M. and Safarpour, H. (2020b), "Frequency characteristics of a GPL-reinforced composite microdisk coupled with a piezoelectric layer", *Eur. Phys. J. Plus*, **135**(2), 144. https://doi.org/10.1140/epjp/s13360-020-00217-x.

Esmailpoor Hajilak, Z., Pourghader, J., Hashemabadi, D., Sharifi Bagh, F., Habibi, M. and Safarpour, H. (2019), "Multilayer GPLRC composite cylindrical nanoshell using modified strain gradient theory", *Mech. Based Des. Struct.*, **47**(5), 521-545. doi/10.1080/15397734.2019.1566743.

Forsat, M., Musharavati, F., Eltai, E., Zain, A.M., Mobayen, S. and Mohamed, A.M. (2021), "Vibration characteristics of microplates with GNPs-reinforced epoxy core bonded to piezoelectric-reinforced CNTs patches", *Adv. Nano Res.*, **11**(2), 115-140. https://doi.org/10.12989/anr.2021.11.2.115.

Ghamkhar, M., Khadimallah, M.A., Iqbal, M.Z., Hussain, M., Yahya, A., Khedher, K.M., Naeem, M.N. and Tounsi, A. (2021), "Performance of FGM bilayered cylindrical shell placed on cantilever edge", *Adv. Nano Res.*, **11**(4), 339-345. https://doi.org/10.12989/anr.2021.11.4.339.

Ghazanfari, A., Soleimani, S.S., Keshavarzzadeh, M., Habibi, M., Assempuor, A. and Hashemi, R. (2020), "Prediction of FLD for sheet metal by considering through-thickness shear stresses", *Mech. Based Des. Struct.*, **48**(6), 755-772. https://doi.org/10.1080/15397734.2019.1662310.

Guo, J., Baharvand, A., Tazeddinova, D., Habibi, M., Safarpour, H., Roco-Videla, A. and Selmi, A. (2021a), "An intelligent computer method for vibration responses of the spinning multi-layer symmetric nanosystem using multi-physics modeling", *Eng. Comput.*, 1-22. https://doi.org/10.1007/s00366-021-01433-4.

Guo, Y., Mi, H. and Habibi, M. (2021b), "Electromechanical energy absorption, resonance frequency, and low-velocity impact analysis of the piezoelectric doubly curved system", *Mech. Syst. Signal Pr.*, **157**, 107723. https://doi.org/10.1016/j.ymssp.2021.107723.

Habibi, M., Darabi, R., Sa, J.C.d. and Reis, A. (2021), "An innovation in finite element simulation via crystal plasticity assessment of grain morphology effect on sheet metal formability", *Proceedings of the Institution of Mechanical*

Engineers, Part L: Journal of Materials: Design and Applications. **235**(8), 1937-1951. https://doi.org/10.1177/14644207211024686.

Habibi, M., Ghazanfari, A., Assempour, A., Naghdabadi, R. and Hashemi, R. (2017), "Determination of forming limit diagram using two modified finite element models", *Mech. Eng*., **48**(4), 141-144. https://doi.org/10.22060/MEJ.2016.664.

Habibi, M., Hashemabadi, D. and Safarpour, H. (2019a), "Vibration analysis of a high-speed rotating GPLRC nanostructure coupled with a piezoelectric actuator", *Eur. Phys. J. Plus*, **134**(6), 307. https://doi.org/10.1140/epjp/i2019-12742-7.

Habibi, M., Hashemi, R., Ghazanfari, A., Naghdabadi, R. and Assempour, A. (2018a), "Forming limit diagrams by including the M–K model in finite element simulation considering the effect of bending", *Proceedings of the Institution of Mechanical Engineers, Part L: Journal of Materials: Design and Applications*, **232**(8), 625-636.

Habibi, M., Hashemi, R., Sadeghi, E., Fazaeli, A., Ghazanfari, A. and Lashini, H. (2016), "Enhancing the mechanical properties and formability of low carbon steel with dual-phase microstructures", *J. Mater. Eng. Perform*., **25**(2), 382-389. https://doi.org/10.1007/s11665-016-1882-1.

Habibi, M., Hashemi, R., Tafti, M.F. and Assempour, A. (2018b), "Experimental investigation of mechanical properties, formability and forming limit diagrams for tailor-welded blanks produced by friction stir welding", *J. Manuf. Proc*., **31**, 310-323. https://doi.org/10.1016/j.jmapro.2017.11.009.

Habibi, M., Mohammadgholiha, M. and Safarpour, H. (2019b), "Wave propagation characteristics of the electrically GNP-reinforced nanocomposite cylindrical shell", *J. Brazil. Soc. Mech. Sci. Eng*., **41**(5), 221. https://doi.org/10.1007/s40430-019-1715-x/

Habibi, M., Mohammadi, A., Safarpour, H. and Ghadiri, M. (2019c), "Effect of porosity on buckling and vibrational characteristics of the imperfect GPLRC composite nanoshell", *Mech. Based Des. Struct*., 1-30. https://doi.org/10.1080/15397734.2019.1701490.

Habibi, M., Mohammadi, A., Safarpour, H., Shavalipour, A. and Ghadiri, M. (2019d), "Wave propagation analysis of the laminated cylindrical nanoshell coupled with a piezoelectric actuator", *Mech. Based Des. Struct*., 1-19. https://doi.org/10.1080/15397734.2019.1697932.

Habibi, M., Safarpour, M. and Safarpour, H. (2020), "Vibrational characteristics of a FG-GPLRC viscoelastic thick annular plate using fourth-order Runge-Kutta and GDQ methods", *Mech. Based Des. Struct*., 1-22. https://doi.org/10.1080/15397734.2020.1779086.

Habibi, M., Taghdir, A. and Safarpour, H. (2019e), "Stability analysis of an electrically cylindrical nanoshell reinforced with graphene nanoplatelets", *Compos. Part B Eng*., **175**, 107125. https://doi.org/10.1016/j.compositesb.2019.107125.

Hashemi, H.R., Alizadeh, A.a., Oyarhossein, M.A., Shavalipour, A., Makkiabadi, M. and Habibi, M. (2019), "Influence of imperfection on amplitude and resonance frequency of a reinforcement compositionally graded nanostructure", *Wave. Random Complex Med*., 1-27. https://doi.org/10.1080/17455030.2019.1662968.

He, X., Ding, J., Habibi, M., Safarpour, H. and Safarpour, M. (2021), "Non-polynomial framework for bending responses of the multi-scale hybrid laminated nanocomposite reinforced circular/annular plate", *Thin Wall. Struct*., **166**, 108019. https://doi.org/10.1016/j.tws.2021.108019.

Hou, F., Wu, S., Moradi, Z. and Shafiei, N. (2021), "The computational modeling for the static analysis of axially functionally graded micro-cylindrical imperfect beam applying the computer simulation", *Eng. Comput*., 1-19. https://doi.org/10.1007/s00366-021-01456-x.

Huang, X., Hao, H., Oslub, K., Habibi, M. and Tounsi, A. (2021a), "Dynamic stability/instability simulation of the rotary size-dependent functionally graded microsystem", *Eng. Comput*., 1-17. https://doi.org/10.1007/s00366-021-01399-3.

Huang, X., Zhang, Y., Moradi, Z. and Shafiei, N. (2021b), "Computer simulation via a couple of homotopy perturbation methods and the generalized differential quadrature method for nonlinear vibration of functionally graded non-uniform micro-tube", *Eng. Comput*., 1-18. https://doi.org/10.1007/s00366-021-01395-7.

Huang, X., Zhu, Y., Vafaei, P., Moradi, Z. and Davoudi, M. (2021c), "An iterative simulation algorithm for large oscillation of the applicable 2D-electrical system on a complex nonlinear substrate", *Eng. Comput*., 1-13. https://doi.org/10.1007/s00366-021-01320-y.

Jaeggi, B., Neuenschwander, B., Schmid, M., Muralt, M., Zuercher, J. and Hunziker, U. (2011), "Influence of the pulse duration in the ps-regime on the ablation efficiency of metals", *Phys. Proc*., **12**, 164-171. https://doi.org/10.1016/j.phpro.2011.03.118.

Jeschke, H.O., Garcia, M.E., Lenzner, M., Bonse, J., Krüger, J. and Kautek, W. (2002), "Laser ablation thresholds of silicon for different pulse durations: theory and experiment", *Appl. Surf. Sci*., **197**, 839-844. https://doi.org/10.1016/S0169-4332(02)00458-0.

Jiao, J., Ghoreishi, S.M., Moradi, Z. and Oslub, K. (2021), "Coupled particle swarm optimization method with genetic algorithm for the static–dynamic performance of the magneto-electro-elastic nanosystem", *Eng. Comput*., 1-15. https://doi.org/10.1007/s00366-021-01391-x.

Khadimallah, M.A., Hussain, M., Naeem, M.N., Taj, M. and Tounsi, A. (2021a), "Monitoring and control of multiple fraction laws with ring based composite structure", *Adv. Nano Res*., **10**(2), 129-138. https://doi.org/10.12989/anr.2021.10.2.129.

Khadimallah, M.A., Hussain, M., Taj, M., Ayed, H. and Tounsi, A. (2021b), "Parametric vibration analysis of single-walled carbon nanotubes based on Sanders shell theory", *Adv. Nano Res*., **10**(2), 165-174. https://doi.org/10.12989/anr.2021.10.2.165.

Kumar, Y., Gupta, A. and Tounsi, A. (2021), "Size-dependent vibration response of porous graded nanostructure with FEM and nonlocal continuum model", *Adv. Nano Res*., **11**(1), 1-17. https://doi.org/10.12989/anr.2021.11.1.001.

Li, J., Tang, F. and Habibi, M. (2020a), "Bi-directional thermal buckling and resonance frequency characteristics of a GNP-reinforced composite nanostructure", *Eng. Comput*., 1-22. https://doi.org/10.1007/s00366-020-01110-y.

Li, Y., Li, S., Guo, K., Fang, X. and Habibi, M. (2020b), "On the modeling of bending responses of graphene-reinforced higher order annular plate via two-dimensional continuum mechanics approach", *Eng. Comput*., 1-22. https://doi.org/10.1007/s00366-020-01166-w.

Liu, H., Shen, S., Oslub, K., Habibi, M. and Safarpour, H. (2021a), "Amplitude motion and frequency simulation of a composite viscoelastic microsystem within modified couple stress elasticity", *Eng. Comput*., 1-15. https://doi.org/10.1007/s00366-021-01316-8.

Liu, H., Zhao, Y., Pishbin, M., Habibi, M., Bashir, M. and Issakhov, A. (2021b), "A comprehensive mathematical simulation of the composite size-dependent rotary 3D microsystem via two-dimensional generalized differential quadrature method", *Eng. Comput*., 1-16. https://doi.org/10.1007/s00366-021-01419-2.

Liu, Y., Wang, W., He, T., Moradi, Z. and Larco Benítez, M.A. (2021c), "On the modelling of the vibration behaviors via discrete singular convolution method for a high-order sector annular system", *Eng. Comput*., 1-23. https://doi.org/10.1007/s00366-021-01454-z.

Liu, Z., Su, S., Xi, D. and Habibi, M. (2020a), "Vibrational responses of a MHC viscoelastic thick annular plate in thermal environment using GDQ method", *Mech. Based Des. Struct.*, 1-26. https://doi.org/10.1080/15397734.2020.1784201.

Liu, Z., Wu, X., Yu, M. and Habibi, M. (2020b), "Large-amplitude dynamical behavior of multilayer graphene platelets reinforced nanocomposite annular plate under thermo-mechanical loadings", *Mech. Based Des. Struct.*, 1-25. https://doi.org/10.1080/15397734.2020.1815544.

Lori, E.S., Ebrahimi, F., Supeni, E.E.B., Habibi, M. and Safarpour, H. (2020), "The critical voltage of a GPL-reinforced composite microdisk covered with piezoelectric layer", *Eng. Comput.*, 1-20. https://doi.org/10.1007/s00366-020-01004-z.

Lutey, A.H., Fortunato, A., Zanini, F. and Carmignato, S. (2016), "Pulsed laser profiling of grinding wheels at normal and quasi-tangential incidence", *Lasers Manuf. Mater. Proc.*, **3**(3), 158-173. https://doi.org/10.1007/s40516-016-0028-5.

Ma, L., Liu, X. and Moradi, Z. "On the chaotic behavior of graphene-reinforced annular systems under harmonic excitation", *Eng. Comput.*, 1-25. https://doi.org/10.1007/s00366-020-01210-9.

Madenci, E. (2021), "Free vibration analysis of carbon nanotube RC nanobeams with variational approaches", *Adv. Nano Res.*, **11**(2), 157-171. https://doi.org/10.12989/anr.2021.11.2.157.

Moayedi, H., Aliakbarlou, H., Jebeli, M., Noormohammadiarani, O., Habibi, M., Safarpour, H. and Foong, L. (2020a), "Thermal buckling responses of a graphene reinforced composite micropanel structure", *Int. J. Appl. Mech.*, **12**(1), 2050010. https://doi.org/10.1142/S1758825120500106.

Moayedi, H., Ebrahimi, F., Habibi, M., Safarpour, H. and Foong, L.K. (2020b), "Application of nonlocal strain–stress gradient theory and GDQEM for thermo-vibration responses of a laminated composite nanoshell", *Eng. Comput.*, 1-16. https://doi.org/10.1007/s00366-020-01002-1.

Moayedi, H., Habibi, M., Safarpour, H., Safarpour, M. and Foong, L. (2019), "Buckling and frequency responses of a graphene nanoplatelet reinforced composite microdisk", *Int. J. Appl. Mech.*, **11**(10), 1950102. https://doi.org/10.1142/S1758825119501023.

Mohammadgholiha, M., Shokrgozar, A., Habibi, M. and Safarpour, H. (2019), "Buckling and frequency analysis of the nonlocal strain–stress gradient shell reinforced with graphene nanoplatelets", *J. Vib. Control*, **25**(19-20), 2627-2640. https://doi.org/10.1177/1077546319863251.

Mohammadi, A., Lashini, H., Habibi, M. and Safarpour, H. (2019), "Influence of viscoelastic foundation on dynamic behaviour of the double walled cylindrical inhomogeneous micro shell using MCST and with the aid of GDQM", *J. Solid Mech.*, **11**(2), 440-453. https://doi.org/10.22034/JSM.2019.665264.

Moradi, Z., Davoudi, M., Ebrahimi, F. and Ehyaei, A.F. (2021), "Intelligent wave dispersion control of an inhomogeneous micro-shell using a proportional-derivative smart controller", *Wave. Random Complex Med.*, 1-24. https://doi.org/10.1080/17455030.2021.1926572.

Najaafi, N., Jamali, M., Habibi, M., Sadeghi, S., Jung, D.w. and Nabipour, N. (2020), "Dynamic instability responses of the substructure living biological cells in the cytoplasm environment using stress-strain size-dependent theory", *J. Biomol. Struct. Dyn.*, 1-12. https://doi.org/10.1080/07391102.2020.1751297.

Oyarhossein, M.A., Alizadeh, A.a., Habibi, M., Makkiabadi, M., Daman, M., Safarpour, H. and Jung, D.W. (2020), "Dynamic response of the nonlocal strain-stress gradient in laminated polymer composites microtubes", *Sci. Rep.*, **10**(1), 1-19. https://doi.org/10.1038/s41598-020-61855-w.

Pourjabari, A., Hajilak, Z.E., Mohammadi, A., Habibi, M. and Safarpour, H. (2019), "Effect of porosity on free and forced vibration characteristics of the GPL reinforcement composite nanostructures", *Comput. Math. Appl.*, **77**(10), 2608-2626. https://doi.org/10.1016/j.camwa.2018.12.041.

Safarpour, H., Ghanizadeh, S.A. and Habibi, M. (2018), "Wave propagation characteristics of a cylindrical laminated composite nanoshell in thermal environment based on the nonlocal strain gradient theory", *Eur. Phys. J. Plus*, **133**(12), 532. https://doi.org/10.1140/epjp/i2018-12385-2.

Safarpour, H., Hajilak, Z.E. and Habibi, M. (2019a), "A size-dependent exact theory for thermal buckling, free and forced vibration analysis of temperature dependent FG multilayer GPLRC composite nanostructures restring on elastic foundation", *Int. J. Mech. Mater. Des.*, **15**(3), 569-583.

Safarpour, H., Pourghader, J. and Habibi, M. (2019b), "Influence of spring-mass systems on frequency behavior and critical voltage of a high-speed rotating cantilever cylindrical three-dimensional shell coupled with piezoelectric actuator", *J. Vib. Control*, **25**(9), 1543-1557. https://doi.org/10.1177/1077546319828465.

Safarpour, M., Ebrahimi, F., Habibi, M. and Safarpour, H. (2020), "On the nonlinear dynamics of a multi-scale hybrid nanocomposite disk", *Eng. Comput.*, 1-20. https://doi.org/10.1007/s00366-020-00949-5.

Shao, Y., Zhao, Y., Gao, J. and Habibi, M. (2021), "Energy absorption of the strengthened viscoelastic multi-curved composite panel under friction force", *Arch. Civil Mech. Eng.*, **21**(4), 1-29. https://doi.org/10.1007/s43452-021-00279-3.

Shariati, A., Habibi, M., Tounsi, A., Safarpour, H. and Safa, M. (2020a), "Application of exact continuum size-dependent theory for stability and frequency analysis of a curved cantilevered microtubule by considering viscoelastic properties", *Eng. Comput.*, 1-20. https://doi.org/10.1007/s00366-020-01024-9.

Shariati, A., Mohammad-Sedighi, H., Żur, K.K., Habibi, M. and Safa, M. (2020b), "On the vibrations and stability of moving viscoelastic axially functionally graded nanobeams", *Materials*, **13**(7), 1707. https://doi.org/10.3390/ma13071707.

Shariati, A., Mohammad-Sedighi, H., Żur, K.K., Habibi, M. and Safa, M. (2020c), "Stability and dynamics of viscoelastic moving rayleigh beams with an asymmetrical distribution of material parameters", *Symmetry*, **12**(4), 586. https://doi.org/10.3390/sym12040586.

Shariati, M., Azar, S.M., Arjomand, M.-A., Tehrani, H.S., Daei, M. and Safa, M. (2020d), "Evaluating the impacts of using piles and geosynthetics in reducing the settlement of fine-grained soils under static load", *Geomech. Eng.*, **20**(2), 87-101. https://doi.org/10.12989/gae.2020.20.2.087.

Shariati, M., Davoodnabi, S.M., Toghroli, A., Kong, Z. and Shariati, A. (2021a), "Hybridization of metaheuristic algorithms with adaptive neuro-fuzzy inference system to predict load-slip behavior of angle shear connectors at elevated temperatures", *Compos. Struct.*, 114524. https://doi.org/10.1016/j.compstruct.2021.114524.

Shariati, M., Faegh, S.S., Mehrabi, P., Bahavarnia, S., Zandi, Y., Masoom, D.R., Toghroli, A., Trung, N.T. and Salih, M.N. (2019), "Numerical study on the structural performance of corrugated low yield point steel plate shear walls with circular openings", *Steel Compos. Struct.*, **33**(4), 569-581. https://doi.org/10.12989/scs.2019.33.4.569.

Shariati, M., Ghorbani, M., Naghipour, M., Alinejad, N. and Toghroli, A. (2020e), "The effect of RBS connection on energy absorption in tall buildings with braced tube frame system", *Steel Compos. Struct.*, **34**(3), 393-407. https://doi.org/10.12989/scs.2020.34.3.393.

Shariati, M., Lagzian, M., Maleki, S., Shariati, A. and Trung, N.T. (2020f), "Evaluation of seismic performance factors for tension-only braced frames", *Steel Compos. Struct.*, **35**(4), 599-609. https://doi.org/10.12989/scs.2020.35.4.599.

Shariati, M., Mafipour, M.S., Ghahremani, B., Azarhomayun, F., Ahmadi, M., Trung, N.T. and Shariati, A. (2020g), "A novel hybrid extreme learning machine–grey wolf optimizer (ELM-GWO) model to predict compressive strength of concrete with partial replacements for cement", *Eng. Comput.*, 1-23. https://doi.org/10.1007/s00366-020-01081-0.

Shariati, M., Mafipour, M.S., Mehrabi, P., Ahmadi, M., Wakil, K., Trung, N.T. and Toghroli, A. (2020h), "Prediction of concrete strength in presence of furnace slag and fly ash using Hybrid ANN-GA (Artificial Neural Network-Genetic Algorithm)", *Smart Struct. Syst.*, **25**(2), 183-195. https://doi.org/10.12989/sss.2020.25.2.183.

Shariati, M., Naghipour, M., Yousofizinsaz, G., Toghroli, A. and Tabarestani, N.P. (2020i), "Numerical study on the axial compressive behavior of built-up CFT columns considering different welding lines", *Steel Compos. Struct.* **34**(3), 377-391. http://doi.org/10.12989/scs.2020.34.3.377.

Shariati, M., Shariati, A., Trung, N.T., Shoaei, P., Ameri, F., Bahrami, N. and Zamanabadi, S.N. (2021b), "Alkali-activated slag (AAS) paste: Correlation between durability and microstructural characteristics", *Constr. Build. Mater.*, **267**, 120886. https://doi.org/10.1016/j.conbuildmat.2020.120886.

Shariati, M., Sulong, N.R. and Khanouki, M.A. (2012), "Experimental assessment of channel shear connectors under monotonic and fully reversed cyclic loading in high strength concrete", *Mater. Des.*, **34**, 325-331. https://doi.org/10.1016/j.matdes.2011.08.008.

Shariati, M., Sulong, N.R., Shariati, A. and Khanouki, M.A. (2016a), "Behavior of V-shaped angle shear connectors: experimental and parametric study", *Mater. Struct.*, **49**(9), 3909-3926. https://doi.org/10.1617/s11527-015-0762-8.

Shariati, M., Sulong, N.R., Shariati, A. and Kueh, A. (2016b), "Comparative performance of channel and angle shear connectors in high strength concrete composites: An experimental study", *Constr. Build. Mater.*, **120**, 382-392. https://doi.org/10.1016/j.conbuildmat.2016.05.102.

Shariati, M., Tahmasbi, F., Mehrabi, P., Bahadori, A. and Toghroli, A. (2020j), "Monotonic behavior of C and L shaped angle shear connectors within steel-concrete composite beams: An experimental investigation", *Steel Compos Struct.* **35**(2), 237-247. http://dx.doi.org/10.12989/scs.2020.35.2.237.

Shokrgozar, A., Safarpour, H. and Habibi, M. (2020), "Influence of system parameters on buckling and frequency analysis of a spinning cantilever cylindrical 3D shell coupled with piezoelectric actuator", *Proceedings of the Institution of Mechanical Engineers, Part C: Journal of Mechanical Engineering Science*. **234**(2), 512-529. https://doi.org/10.1177/0954406219883312.

Stompe, M., Witzendorff, P., Cvetkovic, S., Moalem, A., Stute, U. and Rissing, L. (2012), "Concept for performance-enhancement of ultra-precision dicing for bulk hard and brittle materials in micro applications by laser dressing", *Microelectron. Eng.*, **98**, 544-547. https://doi.org/10.1016/j.mee.2012.07.033.

Tlidji, Y., Benferhat, R., Trinh, L.C., Tahar, H.D. and Abdelouahed, T. (2021), "New state-space approach to dynamic analysis of porous FG beam under different boundary conditions", *Adv. Nano Res.*, **11**(4), 347-359. https://doi.org/10.12989/anr.2021.11.4.347.

von Witzendorff, P., Moalem, A., Kling, R. and Overmeyer, L. (2012), "Laser dressing of metal bonded diamond blades for cutting of hard brittle materials", *J. Laser Appl.*, **24**(2), 022002. https://doi.org/10.2351/1.3685300.

Walter, C., Rabiey, M., Warhanek, M., Jochum, N. and Wegener, K. (2012), "Dressing and truing of hybrid bonded CBN grinding tools using a short-pulsed fibre laser", *CIRP Annals*, **61**(1), 279-282. https://doi.org/10.1016/j.cirp.2012.03.001.

Wang, Z., Yu, S., Xiao, Z. and Habibi, M. (2020), "Frequency and buckling responses of a high-speed rotating fiber metal laminated cantilevered microdisk", *Mech. Adv. Mater. Struct.*, 1-14. https://doi.org/10.1080/15376494.2020.1824284.

Warhanek, M., Walter, C., Huber, S., Hänni, F. and Wegener, K. (2015), "Cutting characteristics of electroplated diamond tools with laser-generated positive clearance", *CIRP Annals*, **64**(1), 317-320. https://doi.org/10.1016/j.cirp.2015.04.010.

Wu, J. and Habibi, M. (2021), "Dynamic simulation of the ultra-fast-rotating sandwich cantilever disk via finite element and semi-numerical methods", *Eng. Comput.*, 1-17. https://doi.org/10.1007/s00366-021-01396-6.

Xiong, Q.M., Chen, Z., Huang, J.T., Zhang, M., Song, H., Hou, X.F., Li, X.B. and Feng, Z.J. (2020), "Preparation, structure and mechanical properties of Sialon ceramics by transition metal-catalyzed nitriding reaction", *Rare Metals*, **39**(5), 589-596. https://doi.org/10.1007/s12598-020-01385-6.

Xu, W., Pan, G., Moradi, Z. and Shafiei, N. (2021), "Nonlinear forced vibration analysis of functionally graded non-uniform cylindrical microbeams applying the semi-analytical solution", *Compos. Struct.*, 114395. https://doi.org/10.1016/j.compstruct.2021.114395.

Yu, X., Maalla, A. and Moradi, Z. (2022), "Electroelastic high-order computational continuum strategy for critical voltage and frequency of piezoelectric NEMS via modified multi-physical couple stress theory", *Mech. Syst. Signal Pr.*, **165**, 108373. https://doi.org/10.1016/j.ymssp.2021.108373.

Zahedi, A., Tawakoli, T., Akbari, J. and Azarhoushang, B. (2014). "Conditioning of vitrified bond CBN grinding wheels using a picosecond laser", *Adv. Mater. Res.*, **1017**, 573-579. https://doi.org/10.4028/www.scientific.net/AMR.1017.573.

Zahedi, A., Tawakoli, T., Azarhoushang, B. and Akbari, J. (2015), "Picosecond laser treatment of metal-bonded CBN and diamond superabrasive surfaces", *Int. J. Adv. Manuf. Technol.*, **76**(5), 1479-1491. https://doi.org/10.1007/s00170-014-6383-5.

Zare, R., Najaafi, N., Habibi, M., Ebrahimi, F. and Safarpour, H. (2020), "Influence of imperfection on the smart control frequency characteristics of a cylindrical sensor-actuator GPLRC cylindrical shell using a proportional-derivative smart controller", *Smart Struct. Syst.*, **26**(4), 469-480. https://doi.org/10.12989/sss.2020.26.4.469.

Zhang, Y., Wang, Z., Tazeddinova, D., Ebrahimi, F., Habibi, M. and Safarpour, H. (2021), "Enhancing active vibration control performances in a smart rotary sandwich thick nanostructure conveying viscous fluid flow by a PD controller", *Wave. Random Complex Med.*, 1-24. https://doi.org/10.1080/17455030.2021.1948627.

Zhao, Y., Moradi, Z., Davoudi, M. and Zhuang, J. "Bending and stress responses of the hybrid axisymmetric system via state-space method and 3D-elasticity theory", *Eng. Comput.*, 1-23. https://doi.org/10.1007/s00366-020-01242-1.

Zhou, C., Zhao, Y., Zhang, J., Fang, Y. and Habibi, M. (2020), "Vibrational characteristics of multi-phase nanocomposite reinforced circular/annular system", *Adv. Nano Res.*, **9**(4), 295-307. https://doi.org/10.12989/anr.2020.9.4.295.

AT